Langevin computer simulations of bacterial protein filaments and the force-generating mechanism during cell division

I. Hörger,[1] E. Velasco,[1,2] J. Mingorance,[3] G. Rivas,[4] P. Tarazona,[1,2,*] and M. Vélez[2]
[1]*Depto. Física Teórica de la Materia Condensada, Universidad Autónoma de Madrid, Madrid 28049, Spain*
[2]*Instituto Nicolás Cabrera, Universidad Autónoma de Madrid, Madrid 28049, Spain*
[3]*Unidad de Investigación y Servicio de Microbiología Hospital Universitario La Paz, Madrid 28046, Spain*
[4]*Centro de Investigaciones Biológicas, Consejo Superior de Investigaciones Científicas, Madrid 28040, Spain*
(Received 23 May 2007; revised manuscript received 25 June 2007; published 7 January 2008)

FtsZ is a bacterial protein that forms filaments that play an essential role in midcell constriction during the process of cell division. The shape of individual filaments of different lengths imaged with atomic force microscopy was modeled considering the protein monomers as beads in a chain and a few parameters to represent their effective interactions. The flexural rigidity and persistence length of the filaments were estimated. This latter value was comparable to the filament length, implying that these biological polymers are halfway between the perfectly stiff linear aggregate whose shapes are fully controlled by the angle between the monomers and highly flexible polymers whose shapes follow a random walk model. The lateral interactions between adjacent filaments, also estimated in the modeling, were found to play an essential role in determining the final shape and kinetics of the coiled structures found in longer polymers. The estimated parameters were used to model the behavior of the polymers also on a cylindrical surface. This analysis points to the formation of helical structures that suggest a mechanism for force generation and amplification through the development of FtsZ spirals at the midcell division point.

DOI: 10.1103/PhysRevE.77.011902 PACS number(s): 87.17.−d, 87.15.−v, 87.10.−e

I. INTRODUCTION

Protein filaments are essential for many aspects of the cellular metabolism, often associated to the generation of mechanical forces within the cell. The best known example is tubulin, a protein present in all eukaryotic cells, which forms the microtubules, hollow cylinders made of 13 adjacent protofilaments [1], with a diameter of 24 nanometers, and a length up to several micrometers. Among other tasks, the microtubules orchestrate the mitosis, with a catch-and-pull nanomachinery which splits each chromosome of the mother cell, and takes exactly one copy of the genetic material to each daughter cell. *In vitro* experiments [2] show the spontaneous self-assembly of the microtubules in bulk solutions of the protein with the guanosine triphosphate (GTP) nucleotide; this molecule has to be attached to the binding site between the protein dimers to form the filaments. Simple physical models of these filaments [3] have helped to understand the peculiar behavior of the growth and shrinkage of these microtubules, produced by the hydrolysis of the GTP molecules to the dephosphorated form guanosine diphosphate (GDP), in what is called the GTPase activity of tubulin. In simple terms, tubulin requires GTP as the "glue" to form the microtubules, and at the same time it "burns" that glue, producing complex growth modes for the aggregates, which can only be maintained with a constant recycling of GDP back into GTP, provided *in vivo* by the cellular metabolism.

The simpler internal structure of bacteria, compared with the complex eukaryotic cells, sets different mechanical problems for their division, and the protein FtsZ plays a prominent role in that respect. At the onset of cell division, in most bacteria and Archaea [4,5], FtsZ localizes at the midcell division site and helps orchestrate the formation of the septosome, a complex structure constituted by several membrane and soluble proteins that induces the cell constriction needed to originate two new independent daughter cells, and most probably provides the mechanical work needed to overcome the osmotic pressure during this process. As in the case of tubulin, the formation of FtsZ aggregates requires the presence of GTP, which is also degradated into GDP at the protein bonds. However, the shape of the polymers formed and their aggregation behavior are quite different. FtsZ polymerizes *in vitro* mainly as single or double stranded filaments whose final shape seems to be highly dependent on the detailed experimental conditions: Straight single-stranded filaments [6], tubules [7], double-stranded filaments [8], and curved and circular forms [9,10] have been described. Ribbonlike higher order structures have also been observed in highly volume occupied conditions emulating the *in vivo* protein environment [11]. Such polymorphism and the observed dynamic behavior indicate that the final shape of the polymer is highly sensitive to environmental conditions such as pH, concentration of GTP, GDP, and several ions, temperature, and other biochemical regulators. A fine modulation of monomer-monomer interaction and the attraction between adjacent filaments probably determines the final shape and dynamic behavior of the polymers. The strength of the association between monomers and the angle between them are related to the presence and phosphorylation state of the nucleotide GTP required for polymerization [9,12], but little quantitative experimental information is yet available [13]. Other physical properties that can provide indirect information about these interactions have not been measured either. The small size of the filaments makes it impossible to obtain

*Corresponding author: pedro.tarazona@uam.es

optical microscopy images from which to measure polymer flexural rigidity, as has been done for their eukaryotic analogs actin and tubulin [14–16].

Recent atomic force microscopy (AFM) experiments have allowed the observation of the dynamic behavior of individual filaments in the presence of GTP [17]. When deposited on mica, they behaved as threadlike dynamic filaments rather than as rigid rods. GTP consumption was accompanied by a substantial structural remodeling. Initially straight filaments bent into flexible open rings that wound into spirals of varying width depending on the number of filaments involved. Fragmentation and reannealing of the initial filaments as well as sliding of the protein monomers and filaments in two dimensions along the mica surface permitted this transformation. GTP hydrolysis was observed to affect the rate of the filament restructuring but not the shape, as the presence of nonhydrolyzable nucleotide analogs also allowed the formation of equivalent structures that were more stable in time. The observed features suggest the superposition of at least four different factors. (i) The formation of polymeric bonds between the FtsZ monomers, leading to filamentary structures. (ii) The existence of a preferred angle between consecutive bonds, along the FtsZ chains, leading to a preferential curvature of the chains. (iii) The fluctuations of the bond angle around that preferred value. (iv) The combination of steric constraint and lateral attraction between the chain segments which are brought close by the coiling of the filament.

Qualitatively different structures would be formed under different relative strengths of these factors, and the present work aims to the analysis of the simplest case: The shape and dynamic behavior of single FtsZ filaments, as observed in AFM images under specific conditions to reduce the coverage of FtsZ protein on the mica surface. We use a coarse-grained modeling of the protein monomers, as beads in a chain, with a reduced set of parameters, like the dependence of the bond free energy with the angle between consecutive links, and the lateral interactions between the chains. Our main concern is to extract quantitative information on the FtsZ protein filaments, from the comparison of AFM images and computer simulations of a chain model, and to use it to explore the possible biological role of the FtsZ protein. The particular values of the model parameters may change with the experimental conditions, but the qualitative conclusions on the mechanism, for the formation of the observed structures, appear to be quite robust.

II. AFM IMAGES OF FTSZ FILAMENTS ON MICA

Figure 1(a) shows a typical AFM image of the curved single FtsZ filaments formed on the mica surface at low surface protein coverage. The protein present in the solution is gradually incorporated into the filaments, and the same surface imaged at a later time shows, in Fig. 1(b), coiled structures that are formed when the filaments have increased in length. In order to reduce the number of variables, the filaments were formed in the presence of GDP-AlF_3, a high affinity analog of the γ phosphate of GTP at the active site of G proteins and microtubules [18] that inhibits the GTPase

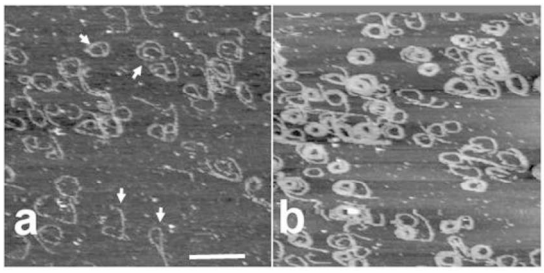

FIG. 1. AFM images of FtsZ filaments formed in the presence of GDP-AlF_3. (a) Image of filaments formed shortly after incorporation of the nucleotide. (b) Same filaments imaged 50 min later showing the shape evolution due to filament growth. Scale bar is 600 nm. The filaments marked with the arrows in (a) are those selected to follow their time evolution in Fig. 7.

activity of FtsZ [19]. The presence of this nonhydrolyzable analog provided stable polymers with no time dependent monomer-monomer interaction in the time scale of the modeling. The whole sample is scanned in about 5 min, which sets our time resolution for the observation of formation and coiling of the FtsZ filaments. The left panel in Fig. 2 presents a partial view of Fig. 1(a), while the central and right panels show the same portion of the mica surface 7 and 13 min later, respectively, covering the main phase of filament growth, and the typical changes in the filament shape over that time scale. As observed in previous experiments with GTP [17], the diffusion of the FtsZ monomers is quite fast to aggregate at the end of the filaments. The slower changes in the shape of the filaments appears to be associated with the interaction between filaments, rather than to any lateral anchoring on the mica surface. To avoid the complex analysis of multifilament networks, we have searched for those filaments which appear isolated from others, over the whole range of AFM images.

Guanine nucleotides GDP and GTP were from Sigma and Roche Molecular Biochemicals, respectively. Other analytical grade chemicals were from Merck or Sigma. *Protein Purification and Assay*.-*Escherichia coli* FtsZ was purified by the calcium-induced precipitation method, and the protein concentration was measured using the BCA assay (Pierce), with spectrophotometrically calibrated FtsZ standards [20].

Atomic force microscopy (AFM) images were taken with a microscope from Nanotec Electrónica (Madrid, Spain) operated in the jump mode [21]. The scanning piezo was calibrated using silicon calibrating gratings (NT-MDT, Moscow, Russia). Silicon nitride tips (DI Instruments) with a force constant of 0.05 N/m were used. A drop of the solution with the FtsZ polymers (formed upon addition of 10 mM GTP to

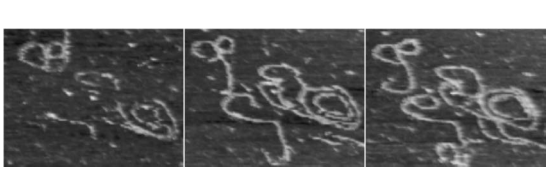

FIG. 2. Time evolution of the FtsZ filaments. The left panel is a portion of the AFM image in Fig. 1(a). The central and right panels show the same surface 7 and 13 min later, respectively.

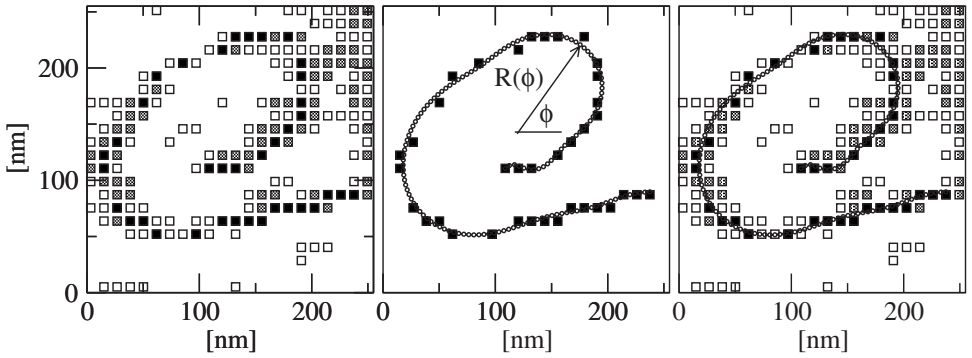

FIG. 3. Example of the data process to get bond-bond angle distribution from the AFM images explained in the text. The panel on the left shows a single FtsZ filament from the AFM image in Fig. 1(a). The black squares are the AFM pixel positions with height over 3 nm, from the flat mica background. The smooth curve in the central and left panels represents the best fit to a polynomial form in polar coordinates, with an optimized choice of the origin (cross). The monomers are assumed to be at regular distances $r_0=4.5$ nm along that curve.

FtsZ protein solutions in Tris 50 mM, *p*H7, 0.5 M KCl, and 5 mM $MgCl_2$ buffer) was incubated over freshly cleaved circular pieces of mica glued onto a Teflon surface. After a few minutes, protein solution was removed and samples washed extensively. Buffer solution containing 10 mM NaF and 0.1 mM $AlCl_3$ was added and, after a few minutes to allow for nucleotide exchange,filaments were imaged. Their evolution and growth was followed for more than 1 h. Images of regions away from the previously scanned surface confirmed that imaging itself did not perturb the polymers. Images were always maintaining the surface under buffer solution.

III. MODEL AND COMPUTER SIMULATIONS

The raw AFM data provide a pixel map $h(x,y)$ with the measured height over the raw mica surface. Under the experimental conditions to observe isolated FtsZ filaments with GDP-AlF_3, the transverse resolution of the map is poorer than the reported results with higher protein coverage and GTP, so that the pixel linear size, $\Delta x=\Delta y\approx 10$ nm, is twice the size of a FtsZ monomer. The vertical resolution is about a factor of 10 better, and the typical height difference between the mica surface and the filaments is about the 5 nm previously reported [17]. Figure 3 presents a typical example of how a single filament shape is extracted from the raw AFM pixel map, without the usual graphic-processing leading to the AFM images in Figs. 1 and 2. The AFM scanning provides the height $h(x,y)$, over the mica surface over a regular square mesh. The left side panel shows the pixels with the largest $h(x,y)$ over a small portion of the image in Fig. 1(a), selected to enclose a single filament. Their filling (white, gray, and black) is correlated with increasing values of $h(x,y)$, and only the black ones, with height above 3 nm, are selected to fit the filament shape as a polynomial function $R(\varphi)$, to describe in polar coordinates the radial distance of each point to a center (x_0,y_0), in terms of the polar angle φ, measured from an arbitrary axis. The least-squares fit is optimized by the appropriate choice of (x_0,y_0), which has to avoid that the function $R(\varphi)$ becomes multivalued. The smooth line in the central panel shows that optimal fit with a polynomial up to order 11, and the discrete positions of the protein monomers, are then assigned along that $R(\varphi)$ curve, keeping the known 4.5 nm distance along the filament. The right side panel shows both the raw AFM data and the extracted filament shape, to give a visual image of the quality of the description.

This procedure is quite robust with respect to the details of the fit, and it works well even for the much longer, and tightly coiled, filaments in Fig. 1(b). As far as the center for the polar coordinates is chosen at the interior of the coil, the function $R(\varphi)$ is a smooth function of the polar angle, which may cover many full rounds. The next step was to model the filaments as a string of beads and to find the energy function which would reproduce the observed features as the thermal equilibrium properties of the chains.

A. Model for short filaments

We first consider an isolated filament formed by N monomers, constrained to the XY plane and linked by spring forces both in the relative distance between adjacent beads, and in the relative angle between consecutive bonds, but without any kind of lateral interaction between the beads. The configuration of the filament is given by the coordinates $\mathbf{r}_i=(x_i,y_i)$ of the $(i=1$ to $N)$ monomers, and the potential energy of each configuration is

$$\mathcal{U}_0[\{\mathbf{r}\}]=\frac{\kappa_0}{2}\sum_{i=1}^{N-1}(|\mathbf{r}_{i+1}-\mathbf{r}_i|-r_0)^2+\frac{\kappa}{2}\sum_{i=2}^{N-1}(\theta_i-\theta_0)^2, \quad (1)$$

where θ_i is the angle between the $(i-1,i)$ and the $(i,i+1)$ bonds. The parameters r_0 and κ_0, associated with the distance between bonded monomers, are easily handled since the mean distance r_0 may be directly set to the known size of the FtsZ monomer ($r_0\approx 4.5$ nm), and the spring constant may be set to be large enough to give a negligible dispersion on the value of $|\mathbf{r}_{i+1}-\mathbf{r}_i|$, but allowing an efficient sampling of the configurations in the computer simulations described below.

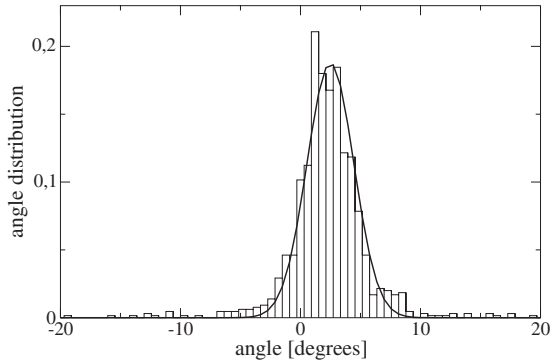

FIG. 4. Distribution of the bond angles in the open FtsZ filaments in Fig. 1 and its Gaussian fit with the parameter in Table I.

The typical shape of the filaments is controlled by the values of the angular spring constant κ, and the preferred angle between monomers θ_0, which establishes the tendency of the chains to be straight (with $\theta_0=0$) or circular, with radius $R_0=r_0/\theta_0$. Such tendency to form circles with fixed radius has been used [10] to explain the formation of aggregates with a sharp size distribution, formed by closed rings energetically stabilized by the formation of the closing bond, and entropically selected as those with $N\approx N_0=2\pi/\theta_0$. However, such arguments do not consider the entropy of the bond angles, i.e., the fluctuations of θ_i around its mean value θ_0. The configurations of relatively short filaments ($N\approx 100$), shown in Fig. 1(a), formed at low protein surface coverage make clear that these fluctuations are important, and in Fig. 4 we present the probability distribution for the bond angles, $\mathcal{P}(\theta_i)$, extracted from the analysis of several short chains without lateral contacts, digitalized as in Fig. 3. Notice that the sign of θ_i has to be referred to a given polarity of the filaments which, as in tubulin or any other protein filament, have two different (plus or minus) extremes. Since the AFM images cannot differentiate between the two ends, we have used the mean curvature along each filament to establish its polarity, arbitrarily defined to have positive mean values of θ_i. The shape of the probability distribution is well represented by a Gaussian, consistent with the thermal equilibrium distribution for the chain energy Eq. (1),

$$\mathcal{P}(\theta_i)=\sqrt{\frac{\beta\kappa}{2\pi}}\exp\left[-\frac{\beta\kappa}{2}(\theta_i-\theta_0)^2\right], \tag{2}$$

with the inverse temperature $\beta=1/(k_BT)$, in terms of Boltzmann k_B constant. The best Gaussian fit to this angle distribution is obtained with a preferential angle $\theta_0\approx 2.5°$, which produces typical filament shapes with that mean curvature, rather than S shapes with null mean curvature. The standard deviation is $\Delta\theta\equiv[\langle(\theta_i-\theta_0)^2\rangle]^{1/2}=(\beta\kappa)^{-1/2}\approx 1.9°$, i.e., $\beta\kappa\approx 890$ at room temperature, or a persistence length $L_P=\beta\kappa r_0\approx 4$ μm. The deviation of $\mathcal{P}(\theta)$ from the Gaussian distribution for $|\theta-\theta_0|>3\Delta\theta$ reflects that the curvature energy flattens from the assumed harmonic potential in $\mathcal{U}_0$, when the bond-bond angle is forced more than 6 or 8° out of its optimal position.

Our estimation for θ_0 is compatible with the interpretation of the sedimentation data [10], with preferential angles producing the closing of chains with $N_0=2\pi/\theta_0\sim 100$. However, with $\Delta\theta\approx\theta_0$ the argument of a preferential chain size controlled by that preferential angle has to be refined, to include the effects of the disorder in the configuration of the chains. It is clear that the typical shapes of the open filaments in Fig. 1 are far from being circular, although they show a clear tendency to have nonzero mean curvature. The angular stiffness κ of the FtsZ filaments is large enough to give (circular) persistent lengths comparable to the chain lengths, especially for the longer filaments formed after the addition of more protein, Fig. 1(b), so that the system is halfway between the perfectly stiff chain ($\beta\kappa\gg N$), with shape fully controlled by θ_0, and the random walk model appropriate for very flexible polymers with ($\beta\kappa\ll N$). It is precisely the intermediate value of $\beta\kappa\sim N$ that makes the role of the lateral interaction between chain segments important, and produces qualitatively different shapes depending on the relative strength of the bending stiffness and the lateral attractions.

B. Long filaments

Modeling the coiled structures observed in Fig. 1(b) required additional consideration. To include the steric repulsions which forbid the chain crossings, and the lateral attractions which promote the formation of ribbonlike structures, we add heuristic Lennard-Jones bead-bead interactions to the ideal chain energy Eq. (1),

$$\mathcal{U}[\{\mathbf{r}\}]=\mathcal{U}_0[\{\mathbf{r}\}]+4\epsilon\sum_{i<j}^{N}\left[\left(\frac{\sigma}{r_{ij}}\right)^{12}-\left(\frac{\sigma}{r_{ij}}\right)^{6}\right], \tag{3}$$

truncated for $r_{ij}=|\mathbf{r}_i-\mathbf{r}_j|\le 2.5\sigma$. The relevant parameters are the distance between filaments σ, for the repulsive core between monomers, which may be directly estimated from the AFM profiles, as the transverse distance between parallel chain segments 12 nm, and the depth of the attractive potential well, ϵ, which can only be estimated through its effects; comparing the equilibrium shapes of the model chains with those observed in the AFM image, Fig. 1(b), from which we select those rolls which are isolated, to avoid the complexity of chain-chain interactions, and represent them as single filaments, with estimated lengths between $N=600$ and 1000.

Since the equilibrium properties of Eq. (3) cannot be obtained analytically, we have explored them through Langevin dynamics simulations (LDS), to represent the overdamped movement of the chain under the viscous friction provided by the liquid bath. The stochastic equations for the velocity of each bead are

$$\frac{d\mathbf{r}_i}{dt}=-\beta D\nabla_i\mathcal{U}[\{\mathbf{r}(t)\}]+\xi_i(t), \tag{4}$$

where the first term is proportional to the total force acting on the bead, with the diffusion constant D of the monomers on the plane; and the second term is a white random noise, with mean squared amplitude $\langle\xi(t)\xi(t')\rangle=kT\delta(t-t')$, to represent the thermal Brownian force induced by the molecular fluctuations of the bath. The natural time scale for the LDS is

TABLE I. Parameters for the model chain energy, Eqs. (4) and (5), used in the Langevin computer simulations.

Description	Value	Source
Monomer length	$r_0=4.5$ nm	AFM [17]
Lateral distance	$\sigma=12$ nm	
Optimal bond angle	$\theta_0=2.5°$	AFM image, Fig. 1(a)
Bending modulus	$\beta\kappa=890$	
Lateral attraction	$\beta\epsilon=2\pm1$	AFM image, Fig. 1(b)
Linear bond spring	$\beta\kappa_0/r_0^2=200$	Optimization of LDS

$t_0=\sigma^2/D$; we use time steps of $10^{-5}t_0$ to integrate Eq. (4) with a simple Euler's forward algorithm. Typically, we run the simulations up to times of $t=10^3t_0$ to get equilibration, and similar times to sample the equilibrium properties. The most relevant conclusions of the present work are based on the thermal equilibrium properties of the system, which do not depend on D, so that they do not require a calibration of t_0. Nevertheless, the order of magnitude $t_0\sim0.1$ s may be roughly estimated from the fact that over times of $t=10^3t_0$ the shapes of short open filaments change in the simulations by similar amounts than those observed in the AFM images taken with 3 min intervals.

We now explore the equilibrium configurations of longer chains $N=600$ monomers using the fixed values of the parameters given in Table I and for different ϵ values. The equilibrium shape of the filaments without lateral attractions would have mean radius $\langle R\rangle=r_0/\theta_0\approx100$ nm; for each value of ϵ we started LDS from spiral configuration with that $\langle R\rangle$, and also with more tightly rolled coils with $\langle R\rangle=60$ nm. In Fig. 5 we present the time evolution of the mean radius for $\beta\epsilon=2$; the gap between the results with different initial structures is closed for $t\approx10^3t_0$. The equilibrium value of $\langle R\rangle$ for that ϵ is 86 nm, with thermal fluctuations of ±2 nm. Similar results were obtained for other values of $\beta\epsilon$; in Fig. 6 we present a typical configuration of the chain, for $\beta\epsilon=1$ and 3. As expected, increasing the lateral attractions produced tighter coils, with larger ratio between the outer and the inner radii: $R_{out}/R_{in}\approx2$ and 3, respectively. That is

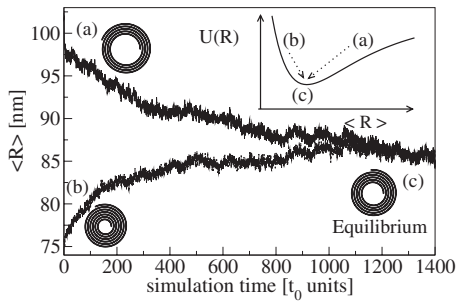

FIG. 5. Filament coil structure along the LDS, described through its mean radius, for our model chain with the parameters in Table I. The two different initial configurations, (a) and (b), evolve to the equilibrium structure (c), which corresponds to small thermal fluctuations around the minimum of the potential energy U, as sketched in the inset.

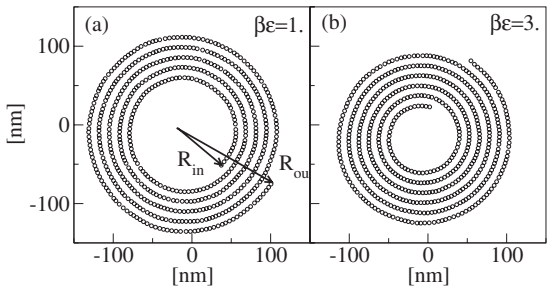

FIG. 6. Typical equilibrium configurations of coils formed in our LDS for two values of the lateral attraction parameter: (a) $\beta\epsilon=1$; (b) $\beta\epsilon=3$. The inner and outer radii are shown in (a).

roughly the range for the ratio R_{out}/R_{in} for the isolated coils in the AFM image, Fig. 1(b), so that we get the semiquantitative estimation of the lateral attraction parameter to be $\beta\epsilon=2\pm1$, within our coarse-grained modeling with the available experimental information.

The main conclusion of this section is that the observed configurations of FtsZ filaments on mica surfaces may be described by a simple interacting-polymer model, Eq. (3), and the comparison of the model LDS and the AFM images gives the quantitative estimation of the model parameters presented in Table I. The most important fact is that the persistence length of the FtsZ filaments is comparable to their typical length, and that gives a particular relevance to the lateral attractions, which produce the characteristic coil shapes observed in the AFM image.

C. Kinetics of coil formation

We may now use the LDS of the model to explore several aspects of the coil formation kinetics, and their possible consequences for the biological role of the FtsZ filaments. Figure 7 presents AFM images of several individual FtsZ filaments from Fig. 1(a), and shows their time evolution as the filaments grow longer and form tightly coiled structures; the LDS with our model help to analyze this process and its dependence with the filament length. In Fig. 8 we present the mean curvature radius for short filaments, starting from straight chain configurations with $N=80$ to 220 monomers. During a first period the chains evolve under the action of the curvature energy $\mathcal{U}_0$, which leads to the optimal radius $R=r_0/\theta_0\approx100$ nm, and to thermal fluctuations around this value. The mean curvature energy per bond is consistently found to be around $kT/2$, and the probability distribution for the bond angles $\mathcal{P}(\theta_i)$, in Eq. (2), may be recovered from the time sampling of each filament. This open-chain regime lasts until a fluctuation produces a first lateral contact along the chain; and the lateral interaction energy, which had been null until that moment, suddenly jumps to a negative value at the same time that the mean radius decreases to $\langle R\rangle\approx50$ nm, with the corresponding increase of the curvature energy. After that sudden change, the chain configuration rapidly evolves toward its thermal equilibrium structure, so that the whole process of the coil formation may be essentially described by the typical time for the formation of the first lateral contact.

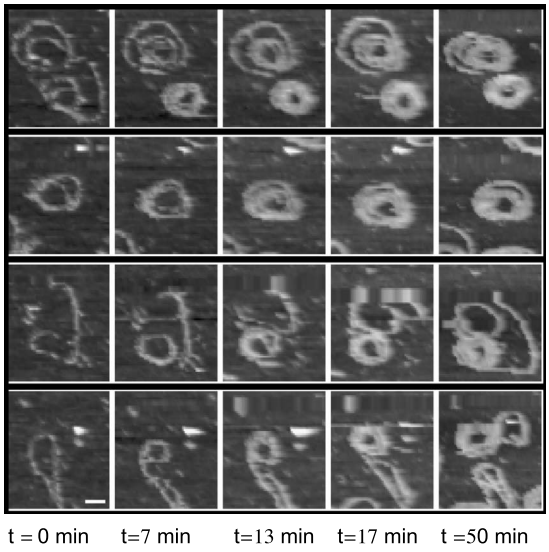

FIG. 7. AFM images of the FtsZ filaments indicated by an arrow in Fig. 1(a). Time zero is the first image taken after addition of GDP-AlF_3. Scale bar is 100 nm.

We have found that the minimal filament coiling time, around $400t_0$, is obtained for chains of 140–150 monomers, i.e., about 0.6 μm of length; for shorter chains the optimal curvature leaves to two ends too distant for the thermal fluctuations to produce the first lateral contact. Thus, for chains with $N=120$, we have found coiling times of $1000t_0$. For longer chains the curvature energy becomes less efficient in driving the chain toward the optimal curvature, since the bending has to correlate the displacements of all the monomers in the chain; and we had times up to $1600t_0$, for $N=200$. Therefore, in a system initially formed by protein monomers, adsorbed on the mica surface, we may expect the growth of short open chains, by independent polymerization reaction controlled by the concentration of GDP-AlF_3. Those chains reaching the length of $N\approx 140$ would be the first to form coils and to decrease their free energy through the formation of lateral contacts. Hence larger filaments with open structures should be very rare, as indeed they appear to be in the AFM image in Fig. 1(b). Once the coils have been formed, the reaction constant for the addition of more monomers would be increased by their lateral interactions, and the available supply of monomers would be preferentially incorporated to the longer coiled filaments, rather than to the remaining open ones; therefore, the filaments with $N\approx 140$ play the role of a critical aggregate in a cooperative nucleation process.

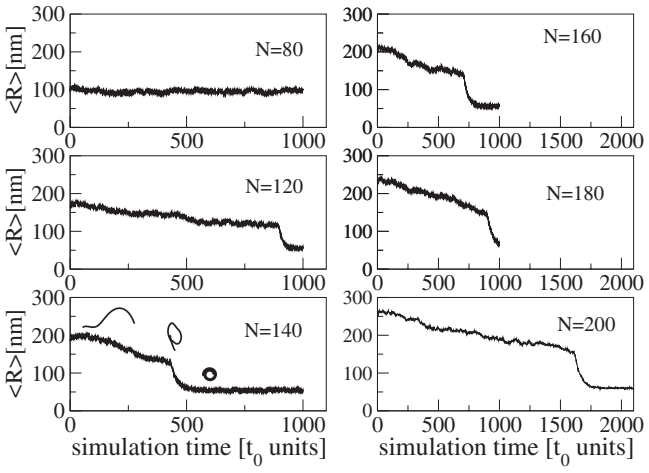

FIG. 8. LDS time evolution of the mean radius for filaments of N monomers, from initially open configurations. The sudden decrease of $\langle R\rangle$ observed for $N\geq 120$ corresponds to the transition to coiled structures, as indicated by the sketched forms over the $N=140$ curve. The typical time for that conformational change depends on the filament length, with a minimum value of $t\approx 400t_0$, in terms of the LDS time scale, obtained for $N\approx 140$. For $N\leq 80$ the filaments remain in the open configuration for all the sampled time. Notice that the time scale is different in the left- and right-hand columns.

The role of the preferential angle θ_0 appears to be of marginal importance for the equilibrium structures; since we may obtain coils like those in Fig. 6 using our chain model with $\theta_0=0$ and larger ϵ, or smaller κ, to overcome the increase of energy to curve preferentially straight chains. However, the kinetics of folding described above is qualitatively changed in the absence of spontaneous bending of the filaments. The thermal fluctuations become very inefficient to produce the first lateral contacts; unless the parameter $\beta\kappa$ is substantially reduced or the length increased. Even in that case, the absence of spontaneous curvature in our simulations produces that, very often, the first lateral contact leads to a hairpin structure, rather than a coil. The double filaments of the hairpin structures are shorter and stiffer than the single strands; their fluctuations are strongly reduced, and their time evolution toward the equilibrium shapes is extremely slow. Therefore, the spontaneous curvature θ_0 is crucial to get easy kinetic paths for the folding of short filaments toward their equilibrium coil structures.

D. Extrapolation to cylindrical geometry

So far, we have described simulations with two-dimensional diffusion of the filaments on a flat surface, since the experimental data to fit our model energy came from the behavior of the filaments on mica. However, our results may be extrapolated to other relevant geometries, at least in a qualitative way, since we do not have quantitative estimations for the bending energy coefficients away from the planar conformations of the AFM experiments. The sedimentation data in bulk solutions [10] would be perfectly compatible with our hypothesis of lateral attraction along the filaments. If we keep the simplest isotropic form for these interactions, and assume that the three-dimensional bending coefficients are not very different from those observed on planar mica substrate, then the most favorable folding of long filaments would lead to toroidal shapes, rather than spirals, and they would be consistent with the observation of a strong cooperative character of the polymerization, and a narrow size distribution for the aggregates in the sediment.

More relevant for the biological function of FtsZ is the extension of the model to a cylindrical support, similar to the

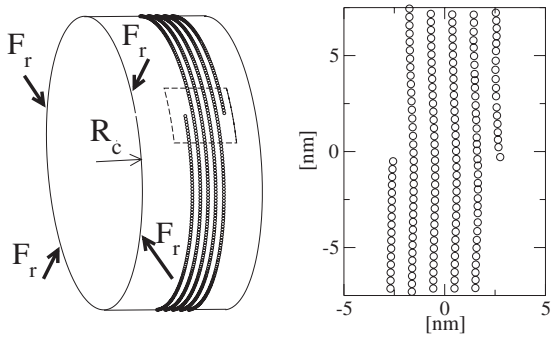

FIG. 9. A helical filament formed by $N=3000$ monomers on a cylindrical surface of radius $R_c=470$ nm, with the energy parameters in Table I. A detailed view of the region within the dashed line is shown on the right-hand side for a typical equilibrium configuration in the Langevin dynamics simulation. The attractive interactions along the filament would produce a radial force F_r on the cylindrical surface as explained in the text.

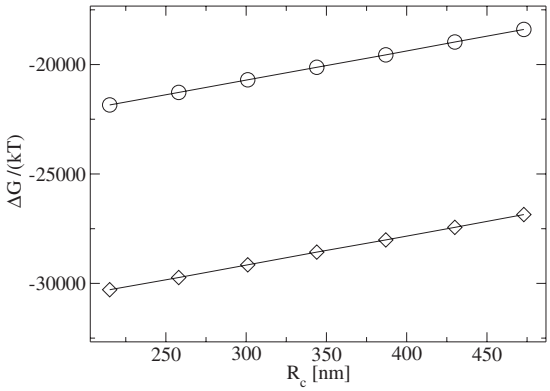

FIG. 10. Mean energy of helical filaments with $N=3000$ (circles) and $N=4000$ (diamonds) monomers on a cylindrical surface of radius R_c, averaged along LD simulations with the energy parameters in Table I.

inner lipid membrane of the bacteria. In that case, the simplest hypothesis is to use exactly the same model interaction, Eq. (3), but to take along one of the axis periodic boundary conditions, with period shorter than the filament length. The FtsZ filaments are formed in the inner side of the lipid membrane, where the FtsZ protein is known to be retained close to the membrane surface through its interaction with the membrane protein ZipA [22] forming dynamic ringlike or helical structures [23–25]; we are aware that the extrapolation of the observed protein-protein interactions on the mica substrate can only provide a rough estimation for the possible interactions in these *in vivo* conditions, but still the qualitative nature of the observed behavior should be both robust with respect to the details and most suggesting for the biological role of the FtsZ protein filaments.

To that effect, we have used Eq. (4) to simulate long ($N=3000$ and 4000) filaments, on cylinders with radius $R_c=200-500$ nm. Much shorter filaments would give exactly the same results as in the simulations on a planar surface, since (within our model) the energy of any configuration would be unchanged if we may cut the cylindrical surface and extend it on a plane, without cutting the filament. Therefore, coiled structures, like those in Fig. 6, would also appear on the cylindrical substrate. However, when the filaments are larger than the perimeter, we observe new configurations which have no counterpart on planar surfaces. If the first lateral contact goes around the cylindrical axis, then the lateral attractions lead rapidly to a helical structure, with the filament coiled on the cylinder, with as many rounds as allowed by its total length, as shown in Fig. 9.

It is remarkable that these predicted helical structures have been observed *in vivo* [24]. From the physical point of view they have a crucial difference with the planar coils; the mean radius of the coils on the planar surface is free to fluctuate around the optimal value which minimizes $\mathcal{U}$; but the radius of the helical ring is imposed by the radius of the cylinder R_c, so that the energy becomes a function $\mathcal{U}(R_c)$, which we have averaged along computer simulations, with different values of R_c, and presented in Fig. 10. With the energy parameters in Table I, the helical filaments are very tight, with rather small fluctuations away from the optimal configuration to get the largest amount of lateral contacts. That gives a very linear increase of $\langle \mathcal{U} \rangle$ with increasing R_c, a radial force

$$F_r = -\frac{d\langle \mathcal{U} \rangle}{dR_c}, \tag{5}$$

produced by the ring on the cylindrical surface, which we find to be of 55 pN, nearly independent of R_c and N, within the values presented in Fig. 9. The effect of stronger lateral interaction between filaments (i.e., larger ϵ), would be an increase of the radial force done by the ring, rather than the change of the shape of the coils as in planar geometry.

IV. DISCUSSION

We have analyzed AFM images of FtsZ filaments formed on the mica surface, in the presence of GDP-AlF_3, by simulating the polymers as chains composed of protein monomers, represented as coarse-grained beads, and taking into account a few parameters to represent the effective interactions between the monomers constituting the polymer chains. Comparison of the global shape of filaments imaged with AFM with the shapes generated by the simulations gave us a quantitative estimate of the preferential angle between monomers θ_0, the relative values of the angular stiffness of the filaments κ, and the energy of interaction between adjacent filaments ϵ. We have to stress the importance of having the first quantitative estimations for the interaction between FtsZ protein monomers, achieved through the contrast between the experimental AFM data and model simulations.

The analysis of short filaments, with open configurations, indicated that in the filaments formed in the presence of the nonhydrolyzable GTP analog GDP-AlF_3 the monomer-monomer angle distribution peaked at $\theta_0 \approx 2.5°$ with a standard deviation of similar magnitude, $\Delta\theta=(\beta\kappa)^{-1/2} \approx 1.9°$. Although the range of angles from 0 to 5° is significantly smaller than the $\theta_0 \approx 20°$ required to form the close circles

described earlier in the presence of GDP [9], it does indicate that GTP can accommodate curved conformations and that GDP is not a requirement for curvature, as had been suggested earlier [12].

The estimated value of $\beta\kappa \approx 890$ at room temperature is equivalent to a flexural rigidity of the filaments of $EI=\kappa r_0 \approx 1.6\times10^{-26}$ N m^2 and a persistence length $L_p=\beta\kappa r_0 \approx 4$ μm. Comparison of these data with previous characterizations of other similar biological polymers underlines the distinctive properties of this bacterial polymer. The mean flexural rigidity of microtubules ranges from 5×10^{-24} N m^2 to 64×10^{-24} N m^2 with a corresponding persistence length of a few millimeters depending on the presence of taxol, GTP, or nonhydrolyzable analog [14,15,26]. Values estimated for labeled actin filaments [14,27] are around 7.3×10^{-26} N m^2 giving a persistence length of $\approx$17.7 μm. The flexural rigidity and the persistence length of the bacterial polymers studied here was found to be about five times smaller than those estimated for labeled actin filaments and several hundred times smaller than that estimated for microtubules. Although the presence of a nonhydrolyzable analog could increase the flexural rigidity estimated in this work, as described for microtubules [15], we have observed qualitatively the same behavior and shape evolution of polymers grown in the presence of GTP (data not shown). Therefore, we may assume that the balance between stiffness and lateral interactions and their effect on the polymer shape is not significantly altered by nucleotide hydrolysis. The functional role of the GTP hydrolysis could be associated with the kinetics of filament rearrangement, but not to the typical equilibrium shapes of the filaments explored here.

The high flexibility of the FtsZ polymers is a most relevant factor for their biological function: During cell division the septal ring has to accommodate, or induce, the changes in cell diameter associated with the cell constriction. Our model suggests that the typical length of the filaments is tuned to get a balance with their flexibility, $\beta\kappa \sim N$, which gives a relevant role to the lateral attractive interactions in the stabilization of compact ordered coils, qualitatively different of the disorder globular structures formed by flexible polymer chains (with $\beta\kappa \ll N$). On the opposite end, much stiffer aggregates with $\beta\kappa \gg N$ would aggregate under the effects of the lateral attractive interaction, but without significant change in their individual conformations. The strong sensitivity of the FtsZ aggregates to the biochemical conditions of growth is probably a result of the great plasticity provided by that close balance, which may be easily shifted toward one or the other side by small changes in the chemical environment.

In our LDS we have found that the joint effect of the preferential curvature and the low flexural rigidity lead to a crucial effect of the lateral attractions in the typical shapes of chains with more than 100 monomers, i.e., for FtsZ filaments larger than about 0.5 μm. The estimated value of the attractive energy per lateral contact is $\beta\epsilon=2\pm1$, or around 5 kJ/mol, equivalent to the energetic cost of bending a bond 4° away from its preferential angle. That gives a clear picture of the close balance between the flexural energy and the optimization of the lateral contacts. Also, it is useful to compare ϵ with the only known experimental estimation of the bond energy $\Delta G \approx 37$ kJ/mol (or $\beta\Delta G \approx 16$) in Ref. [13], corresponding to an FtsZ from the thermophilic archaea it Methanococcus jannaschii for experiments carried out at 55 °C. The ratio $\Delta G/\epsilon > 8$, is consistent with the description of the FtsZ filaments as "linear aggregates," with a hierarchical structure in which the lateral attractions are important, but significantly weaker than the bond energy between monomers along the filament. Previous reports had already suggested the possible biological relevance of lateral interactions between filaments. Ribbonlike structures formed under experimental conditions that simulate the crowded interior of the cell indicate that higher order structures formed through lateral interactions between filaments are favored under conditions that emulate the ones found *in vivo* [11].

The simulations of coil formation kinetics using the determined filament parameters indicate that the spontaneous curvature of the filaments accelerates the formation of coiled structures. The lateral interactions now play the role of facilitating the addition of monomers to the coiled filaments over the remaining open ones. This cooperative nucleation process observed in two dimensions due to the presence of lateral interactions would also manifest in the toroidal structures predicted to form in bulk solution. This finding is consistent with the observed cooperative behavior of the polymerization process [13,28] and provides further support to the suggestion that this cooperativity is due to an alternative polymerization mechanism of these curved and coiled polymers and not due to the presence of double stranded filaments, as is the case for actin [10].

Simulations that explore the shape of the polymers formed on a cylinder indicate the formation of a cylindrical helix when their length becomes equal to the circular perimeter. The helical folding represents an easy to reach, and hard to remove, metastable state for long filaments, which have the right topology to perform the most likely biological function of the FtsZ protein, forming the FtsZ rings. The shape of the helical structures is essentially fixed by the radius of the cylindrical support, instead of being a balance between the curvature energy and the lateral attractions, as in the case of the spirals observed on a flat surface. The lateral attraction between filaments has an interesting consequence in this helical configuration: It can create a force on the cylindrical surface. The order of magnitude of this force comes from the energy ($\epsilon \approx 10^{-20}$ J) of an optimal lateral contact, divided by the monomer size $r_0 \approx 5$ nm, i.e., about 20 pN, well within the range of forces expected for biological motors [29]. This possibility had not been contemplated among the previously suggested molecular mechanisms of *Z* ring constriction during septum formation. Suggestions that FtsZ subunits released from the ring reducing the diameter of the ring or filaments sliding against each other without disassembling, as occurs in the actomyosin ring in eukaryotes [7], had been put forward, but none of them were based on quantitative experimental evidence that allowed an estimation of the possible forces involved. This proposed force-generating mechanism does not require the presence of other proteins and relies exclusively on the interaction between FtsZ monomers when they are free to distribute on a surface. One experimentally testable prediction of our results is that mutations, biochemical modulation, or interaction with other proteins that

affect the lateral interaction between filaments could affect the constriction process. Indeed, it has been reported [30] that FtsZ mutations affecting the surface involved in lateral interactions between filaments were not able to support cell division, suggesting that the lateral surfaces of the protofilaments are important for the protein function.

In summary, we have estimated the preferential angle between monomers, the flexural rigidity of FtsZ filaments, and found that their lateral interactions are important in determining the final shape of the polymers. The predicted helical structure of such polymers formed on a cylindrical surface suggests a mechanism for force generation and amplification that could contribute to the formation of the constriction required for cell division.

ACKNOWLEDGMENTS

This work has been supported by the Dirección General de Investigación of Spain, under Grant Nos. FIS2004-05035-C03-02 and BFU2005-04087-C02, and the Comunidad Autónoma de Madrid under Grant No. S-0505/ESP-0299.

[1] A. Desai and T. J. Mitchinson, Annu. Rev. Cell Dev. Biol. **13**, 83 (1997).
[2] H. P. Erickson, Annu. Rev. Biophys. Biomol. Struct. **21**, 145 (1992); F. J. Nedelec, T. Surrey, A. C. Maggs, and S. Leibler, Nature (London) **389**, 305 (1997).
[3] M. Dogterom and S. Leibler, Phys. Rev. Lett. **70** 1347 (1993); H. Flyvbjerg, T. E. Holy, and S. Leibler, *ibid.* **73**, 2372 (1994).
[4] M. Vicente, A. I. Rico, A. I. Martí, and J. Mingorance, J. Bacteriol. **188**, 19 (2006).
[5] L. Romberg and P. A. Levin, Annu. Rev. Microbiol. **57**, 125 (2003).
[6] L. Romberg, M. Simon, and H. Erickson, J. Biol. Chem. **276**, 11743 (2001).
[7] D. Bramhill and C. M. Thompson, Proc. Natl. Acad. Sci. U.S.A. **91**, 5813 (1994).
[8] M. A. Oliva, S. Huecas, J. M. Palacios, J. M. Martí, J. M. Valpuesta, and J. M. Andreu, J. Biol. Chem. **278**, 33562 (2003).
[9] H.P. Erickson, D.W. Taylor, K.A. Taylor, and D. Bramhill, Proc. Natl. Acad. Sci. U.S.A. **93**, 519 (1996).
[10] J.M. Gonzalez, M. Vélez, M. Jimémez, C. Alfonso, P. Schuck, J. Mingorance, M. Vicente, A.P. Minton, and G. Rivas, Proc. Natl. Acad. Sci. U.S.A. **102**, 1895 (2005).
[11] J. M. González, M. Jiménez, M. Vélez, J. Mingorance, J. M. Andreu, M. Vicente, and G. Rivas, J. Biol. Chem. **278**, 37664 (2003).
[12] J. F. Díaz, A. Kralicek, J. Mingorance, J. M. Palacios, M. Vicente, and J. M. Andreu, J. Biol. Chem. **276**, 17307 (2001).
[13] S. Huecas and J. M. Andreu, J. Biol. Chem. **278**, 46146 (2003).
[14] F. Gittes, B. Mickey, J. Nettleton, and J. Howard, J. Cell Biol. **120**, 923 (1993).
[15] P. Venier, A. C. Maggs, M. F. Carlier, and D. Pantolini, J. Biol. Chem. **269**, 13353 (1994).
[16] A. Ott, M. Magnasco, A. Simon, and A. Libchaber, Phys. Rev. E **48**, R1642 (1993).
[17] J. Mingorance, M. Tadros, M. Vicente, J. M. González, G. Rivas, and M. Vélez, J. Biol. Chem. **280**, 20909 (2005).
[18] J. Bigay, P. Deterre, C. Pfiste, and M. Chabre, EMBO J. **6**, 2907 (1987).
[19] D. RayChaudhuri and J.T. Park, J. Biol. Chem. **269**, 22941 (1994).
[20] G. Rivas, A. López, J. Mingorance, M. Ferrandiz, S. Zorrilla, A. Minton, M. Vicente, and J. M. Andreu, J. Biol. Chem. **275**, 11740 (2000).
[21] F. Moreno-Herrero, P. J. de Pablo, R. Fernández-Sánchez, J. Colchero, J. Gómez-Herrero, and A. Baró, Appl. Phys. Lett. **81**, 2620 (2002).
[22] C. A. Hale and P. A. J. de Boer, Cell **88**, 175 (1997).
[23] X. Ma, D. W. Ehrhardt, and W. Margolin, Proc. Natl. Acad. Sci. U.S.A. **93**, 12998 (1996).
[24] S. Thanedar and W. Margolin, Curr. Biol. **14**, 1167 (2004).
[25] J. Stricker, P. Maddox, E. D. Salmon, and H. P. Erickson, Proc. Natl. Acad. Sci. U.S.A. **99**, 3171 (2002).
[26] B. Mickey and J. Howard, J. Cell Biol. **130**, 909 (1995).
[27] R. Yasuda, H. Miyata, and K. Kinosita, Jr., J. Mol. Biol. **263**, 227 (1996).
[28] L. Romberg, M. Simon, and H. P. Erickson, J. Biol. Chem. **276**, 11743 (2001).
[29] K. Kinbara and T. Aida, Chem. Rev. **105**, 1377 (2005).
[30] Ch. Lu, J. Stricker, and H. P. Erickson, BMC Microbiol. **1**, 1471 (2001).